Laboratory study on the propagation of edge cracks in rock-like material and its implication in coal mining

Baoliang Zhang [a,b], *Shichuan* Zhang [a*] , and *Qingshuang* Zhao[b]

[a] State Key Laboratory of Mining Disaster Prevention and Control, Shandong University of Science and Technology, Qingdao, 266590, China
[b] School of Architecture and Civil Engineering, Liaocheng University, Liaocheng 252000, China

Abstract. Rock fracture propagation is a major hazard for mining and tunnel excavation in fractured rock masses or coal seams. A longwall mining panel with a typical dimension of 200m (width)×1000m (length)×3m (height) can be considered as an open edge crack. The fracturing processes in the vicinity of the edge crack (or the longwall panel) particularly in the roof and floor are critically important for the safety of mining operation because fracturing can lead to water inrush and dynamic loading on the working face. It's therefore important to understand and predict the pre-existing edge crack initiation and propagation in rock masses. This paper describes a study investigating the mechanisms and pathways of rock fracture under uniaxial compression. In this study, a rock-like material which consists of model gypsum, water and diatomaceous earth at a mass ratio of 165:75:2 was used. The uniaxial compression strength of the material decreased with the increase of the length of pre-existing edge crack. During the tests, wing (tensile) cracks were first observed at the tip of the pre-existing edge crack. This was followed by secondary cracks as the loading increased. The final failure of the specimens however was dominated by tensile cracks throughout the specimens. Due to the sudden crack initiations in the specimens, the loading stress in the specimen varies stepwise, and acoustic emission (AE) energy and amplitude showed abrupt changes when crack initiated. When the crack initiation occurred, the loading stress of the specimens showed a notable retreat in the stress-strain curve, and the recorded AE energy and amplitude showed a sharp spike. These findings from this experimental study have been applied to the underground longwall mining to explain the failure mechanisms in the floor of the mining panel. The fracturing process associated with the pre-existing edge crack resembles the formation of flow channels for water inrush during longwall mining.

1 Introduction

Rock fracture propagation is one of the key concerns in many rock engineering problems (Shen et al. 2016, 2020; Feng et al. 2019b) because it could lead to rock mass instability

* Corresponding author: 373260186@qq.com

and rapid increase of water inflow. For deep underground coal mines using the longwall mining method, a major safety issue is the water inrush from the aquifers above or below the mining horizon（Zhang et al. 2017, 2019）. Water inrush is often induced by the fracturing of the aquitard rock layer between the highly pressurized aquifer and the mining seam. Understanding and predicting the fracturing process in the roof and floor of the mining seam is therefore critically important for the hazard management of water inrush (Sun et al. 2017). A typical longwall mining panel is often 200-300m wide, 0-1000m long, and 2-4m height. Due to its relatively thin height, it may be considered as an open edge crack under the compressive stress (overburden stress). With this simplification, the rock fracturing processes in the roof and floor of a longwall panel can then be investigated in laboratory using specimens containing edge cracks under uniaxial compression.

Over the past several decades, a large number of studies have been performed to investigate the fracture mechanical behaviors of pre-existing cracks. Crack initiation and propagation in two-dimension have been investigated using different materials (Feng et al. 2019a). Cracks or geological structures such as the faults and joints can seriously affect rock body's strength and stability. When loaded, the cracks within the rock material may deform slide, propagate and coalesce. As 2D crack is easier for theoretical study, numerical modeling and experimental observation, many researchers investigated the 2D crack extension mechanisms. SMITH (1981) studied the propagation process and monitoring method for edge crack within semi-infinite solid material under pressure, and found that stress intensity factor changes with crack length. Segall (1984) found that tension crack is the main cause of the deformation and failure of laboratory specimen, during studying the extension of Type I open crack. Shen et al (1995) used gypsum specimen with prefabricated cracks to study the crack propagation mechanism and rock bridge failure process under uniaxial compression, and the results showed that different geometric sizes of crack cause different stress conditions and failure modes in the rock bridge region. Reyes et al (1991) studied the mechanism of crack propagation and rock bridge breakage under different crack geometry. Zhao et al (2008) characterized the failure of biotite gneiss and granite specimens with pre-existing cracks (edge crack with length of 5mm) under compressive loading, and according to results, shear failure occurred in the rock specimens with pre-crack and splitting failure occurs in the intact rock. Xue et al (2002) used a sheet test specimen from PMMA polymer transparent material, with 3 and 4 parallel edge cracks on either side, and then employed high speed camera to capture the tension cracks developed at the tip of the pre-crack and then the tension fails were found in whole specimen until the final failure of the whole specimen.

In selection of materials, Wong et al (2006), Zhu et al (2016), Xue et al (2002) and others used transparent PMMA to simulate brittle rock. The biggest advantage of this method is that it is easier to observe the path of crack propagation, but PMMA behaves quite differently from real rock particularly on the aspect of shear fracture propagation. Regarding study method, Luis et al (2013), Shen et al (2011) and Tang (2007) used numerical simulation software to simulate the failure process of rock with pre-existing cracks, and revealed the propagation mechanism of Mode I (the opening mode), Mode II (the edge-sliding mode), Mode III (the tearing mode). To observe rock failure process, researchers have adopted technologies like acoustic emission, high-speed camera and computer tomograghy (CT) etc. Zhao et al (2015) developed an image analyzing software to characterize the deformation and failure of rock-like materials with a single pre-existing crack. Li et al (2007), Li et al (2005), Chen et al (2005), Yang et al (2007) and others used CT scanning technology to study the extension mechanisms of 3D crack, intermittent crack and crack in rock specimen. So far, most of these studies were focused on the mechanisms of crack propagation. It has not been found that any of the previous studies were focused on using the edge cracks to investigate the seam roof and floor fracturing in coal mining.

On the aspects of testing material selection, monitoring method and numerical simulation of crack extension, existing studies focus on the propagation mechanism of crack coalescence and contained 3D cracks, with few studying on the edge crack extension

of rock materials. This paper explores the propagation characteristics of edge cracks under compressive loading and explains how the seam floor of a mining panel fails during mining. The mining progress was simulated by using the pre-existing edge cracks with different lengths, simulating the increasing panel length during longwall mining. Brittle material made of gypsum and water was used to simulate the real rock behavior in the mining environment. The results hence will be directly relevant to the seam floor water inrush and its prevention.

2 Testing Material and Method

2.1 Testing Material

Using the real rock from field, although highly desirable, has a lot of difficulties. During the specimen preparation, the vibration from rock cutting to prepare the specimen and the cracks is likely to destruct the specimen. In addition, using country rock will lead to high variation of the testing results, making it difficult to observe the mechanisms. For this reason, rock-like material was used to simulate the process of crack propagation instead. The testing material was a mixture of model gypsum, diatomite and water (30℃), with a ratio of each ingredient as 165: 2: 75 by weight. The material has a Young's modulus of 4.3GPa of tensile strength of 2.4Mpa. This material can effectively simulate the crack propagation process in brittle rock.

The specimen was taken a cuboid, with a dimension of 100mm (L) × 100mm (W) × 200mm (H). The cracks were located horizontally at the middle height of the specimen on the left, with a length of 100mm and three different width of 30mm, 40mm and 50mm, respectively. The height (or thickness) of the specimen is shown as Figure 1.

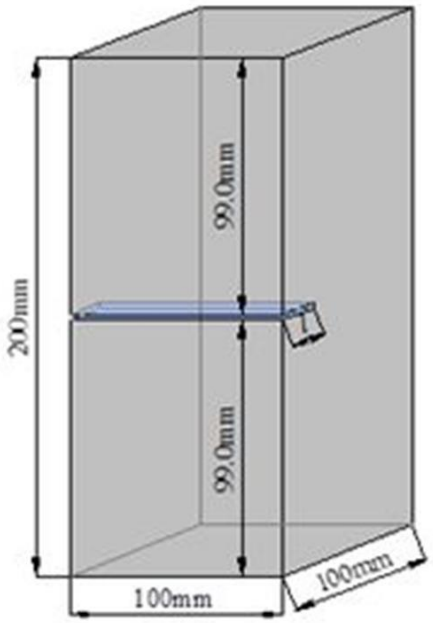

Fig. 1. Test Design (in mm). Note: the crack width *l* in this test included 3 arrangements as 30mm, 40mm and 50mm

2.2 Test Method

The testing instruments mainly included test loading system, acoustic emission monitoring system and a video camera. The loading system used was the RLJW-2000 servo controlled rock pressure testing system which uses piston driven by servo-controlled motor to pump high pressure oil into the loading oil tank for applying and controlling axial pressure (or displacement), with a maximum axial pressure 2,000kN and maximum axial displacement 100mm at accuracy of ±1%. The test was loaded by controlling displacement at 0.003mm/min.

The acoustic emission monitoring device used was MISTRAS series PCI-2 acoustic emission monitoring and analysis system which monitors crack propagation dynamically and in real time. The system has with a threshold of 40dB, floating threshold of 6dB (when ambient noise is smaller than 20dB), and average wave speed of 2,286m /s and 6-channel location. Before testing, the specimen was underwent material acoustic characteristic matrix tests. During testing, the tip of the probe and the contact between the specimen and the pad were evenly applied with vaseline for reflection effect and its interference to sound signal emission, to ensure that the emitted sound signals can be well received by the sensor. The acoustic emission probes were mounted on the specimen with adhesive tape and the sensitivity test was carried out for the sensors before testing, to ensure that the signal magnitude captured by every probe is more than 90dB.

A SONY camcorder was used to capture the propagation process of surface crack. The main control and monitoring system for testing is shown as Figure 2. During testing, the loading system, the acoustic emission system and the camcorder were activated and synchronized for the same timing, in order to process data and analyze the closure, initiation and propagation of cracks.

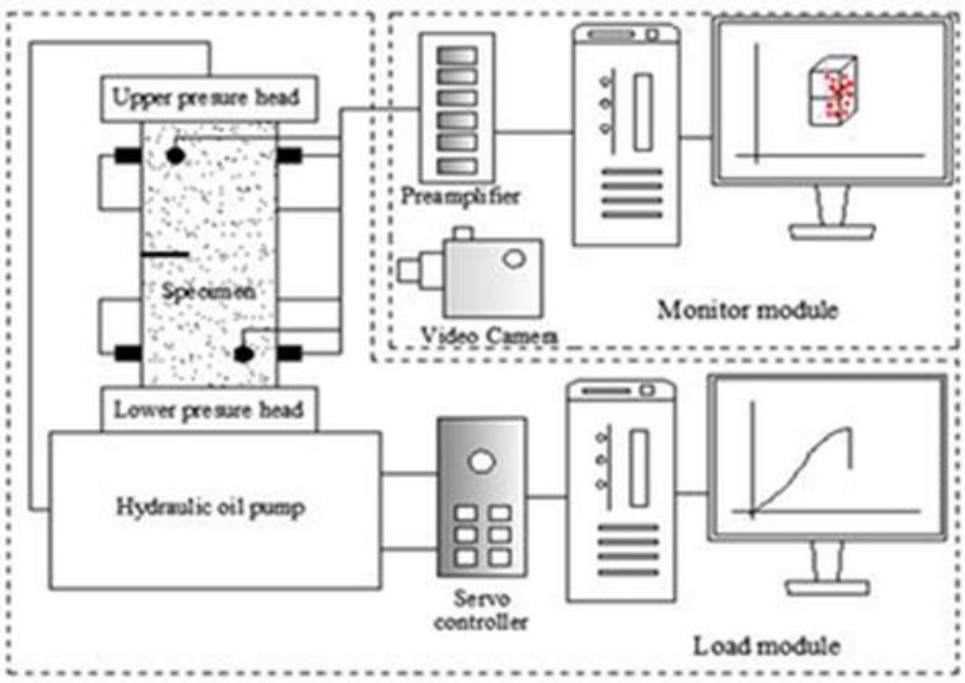

Fig. 2. Loading and Monitoring System for testing

3 Test Result Analyses

3.1 Analyzing Propagation characteristics of Surface Crack

During loading, the tip of the open edge pre-crack had higher stress concentration than other parts of the specimen, so that the new crack started at the tip of the pre-existing crack. The propagation processes of various groups of surface cracks are shown in Figures 3-5, and the resulted crack types shown as Table 1.

Table 1. Crack Types in Specimens

No.	**Crack type**	**Stress level**
P*ref*1	Pre-existing Edge Crack	0
Crack A1	Wing Tension Crack	12.5MPa
Crack A2	Anti-wing Tension Crack	14.9MPa
Crack A3	Secondary Tension Crack	14.9MPa
P*ref*2	Pre-existing Edge Crack	0
Crack B1	Anti-wing Tension Crack	2.5MPa
Crack B2	Secondary Tension Crack	9.7MPa
P*ref*3	Pre-existing Edge Crack	0
Crack C1	Wing Tension Crack	3.6MPa
Crack C2	Anti-wing Tension Crack	5.8MPa
Crack C3	Anti-wing Tension Crack	6.3MPa
Crack C4	Secondary Tension Crack	7.5MPa

(1) When crack width l=30mm as exemplified in specimen 1-1, the propagation process is shown as Figure 3.

At the early stage of loading, the pre-existing crack closed and its tip appeared scaling off under gradually increasing load. When the load increased to 12.5 MPa or about 83.89% of peak strength, a macro-crack started from the tip of the pre-existing crack and propagated rapidly in an angle of 86° from the horizontal direction to the upper end of the specimen, resulting in a wing tension crack A1. When the load reached to the specimen's peak strength of 14.9MPa, an anti-wing tension crack A2 appeared from the tip of the pre-existing crack, with the propagation direction close to the direction of loading. At the same time, a secondary tension crack A3 began from the lower face of the specimen. The specimen mainly suffered from tension failure.

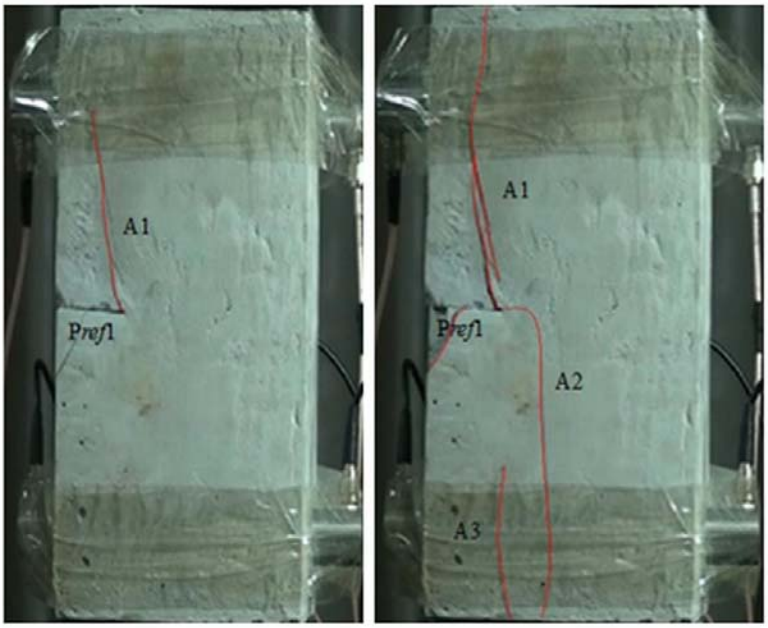

(a) 12.5 MPa (b) 14.9 MPa

Fig. 3. Crack Propagation Process in Specimen 1-1

(2) When crack width l=40mm as exemplified in specimen 2-1, the propagation process is shown as Figure 4.

When the load increased to 2.5 MPa or about 25.77% of the peak strength, a Mode I crack started from the tip of the specimen and rapidly connected to its lower end of the specimen, forming an anti-wing tension crack B1, with the propagation direction perpendicular to the pre-existing crack. When the load reached to 9.7MPa which is the peak strength of the specimen, a secondary tension crack B2 started from the tip of the pre-existing crack, propagated in the loading direction and finally merged with the anti-wing tension crack B1, while the specimen totally disintegrated from tension failure.

(3) When crack width l=50mm as exemplified in specimen 3-2, the propagation process is shown as Figure 5.

When the load increased to 3.6MPa or about 48% of the peak strength, a marco wing tension crack C1 developed from the tip of pre-existing edge crack, with an initiation angle and propagation angle of 78° and 90°. When the load increased to 5.8MPa and 6.3MPa, anti-wing tension crack C2 and C3 developed upward and downward from the tip of the pre-existing crack in an angle of 90°. When the load reached to the peak strength of 7.5MPa, secondary tension crack C4 developed on the specimen and the specimen again was disintegrated by tension failure.

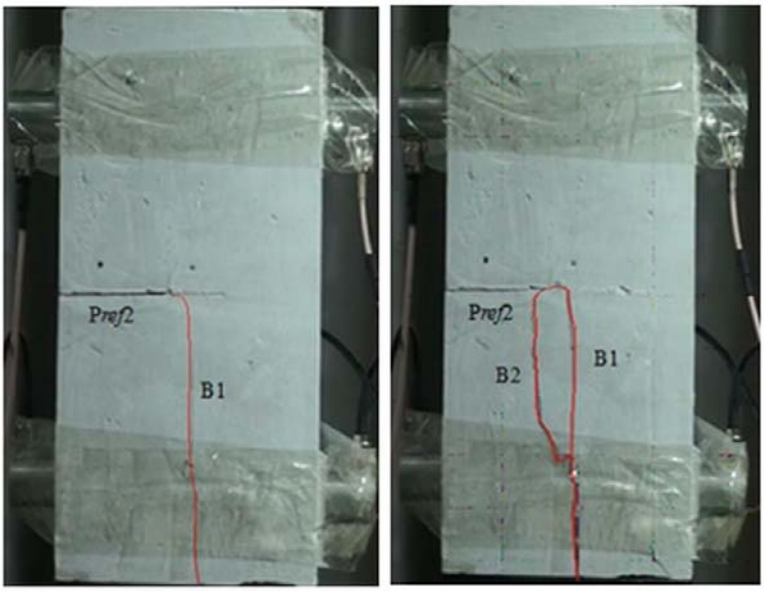

(a) 2.5 MPa (b) 9.7 MPa

Fig. 4. Crack Propagation Process in Specimen 2-1

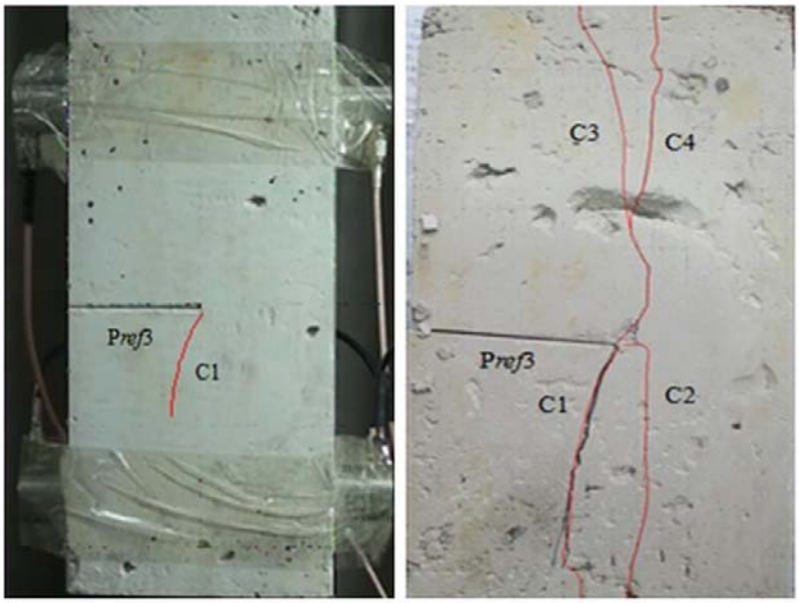

(a) 3.6 MPa (b) 7.5 MPa

Fig. 5. Crack Propagation Process in Specimen 3-2

Notes: the Pef1~Pef3 (Pre-existing Fracture) are pre-existing edge cracks with width respectively as 30mm, 40mm and 50mm in figures 3-5.

The crack initiation strength and uniaxial compressive strength of specimens are summarized in Table 2. According to Table 2, the crack initiation strength and average uniaxial compressive strength decrease with increasing width of the pre-existing edge crack. When their width increasing from 30mm to 50mm, the average crack initiation strength reduces from 11.3MPa to 1.5MPa and the strength specimen peak strength ratio reduces from 14.2MPa to 7.6MPa. The ratio of crack initiation strength to peak strength reduces from 0.79 to 0.19.

Table 2. Cracking Strength and Uniaxial Compressive Strength

No.	Pre-existing edge crack width *l*/mm	Cracking strength /MPa	Uniaxial compressive strength /MPa	Strength ratio	Average cracking strength /MPa	Average uniaxial compressive strength /MPa
1-1	30	12.5	14.9	0.84	11.3	14.2
1-2	30	10.3	13.6	0.76		
1-3	30	11.1	14.2	0.78		
2-1	40	2.5	9.7	0.26	3.1	10.4
2-2	40	3.3	10.8	0.31		
2-3	40	3.4	10.7	0.32		
3-1	50	2.2	8.3	0.27	1.5	7.6
3-2	50	0.3	7.5	0.04		
3-3	50	1.9	7.1	0.27		

3.2 Analysis of Acoustic Emission Characteristics

Figure 6 (a) to (c) shows the acoustic emission characteristics of specimens with difference crack widths under the effect of uniaxial pressure. When crack width l=30mm, the typical AE results are exemplified by channel 1 in specimen 1-1. The stress-time-energy curve and the stress-time-magnitude curve have been analyzed, with results shown in Figure 6 (a). When the wing tension crack A1 started, the AE energy and the magnitude was 20,448 and 99dB respectively, and the stress has a moderate but notable sudden drop. When the loading stress reached the peak strength of the specimen, anti-wing tension crack A2 and secondary tension crack A3 appeared, while the AE energy rapidly climbed to 34,528 and the magnitude became >100 dB (note that a measuring range of set to 40-100, hence magnitude greater than 100dB was not reflected). When crack width l=40mm as represented by the channel 1 in specimen 2-1, the stress-time-energy curve and the stress-time-magnitude curve have been analyzed, as shown in Figure 6 (b). When the wing tension crack B1 started, the energy value was 17,829 and the stress had a small sudden drop. When the loading time reached 1,576s, stress had a major drop, and the energy value jumped up to 59,535, but no surface crack was observed. When stress reached the peak strength of 7.5MPa of the specimen, secondary tension crack B2 appeared, and the AE energy value climbed rapidly to 18,517. When crack width l=50mm as exemplified by the channel 1 in specimen 3-2, the stress-time-energy curve and the stress-time-magnitude curve are shown in Figure 6 (c). When crack C1 initiated, the AE energy was respectively 11547, and the stress began to fluctuate. With load increasing, crack C2 and C3 started, causing stress, AE energy and magnitude to change suddenly. When peak stress was applied on the specimen, secondary tension crack C4 started, causing the AE energy and the magnitude to abruptly change to 14,797 and 98 dB respectively.

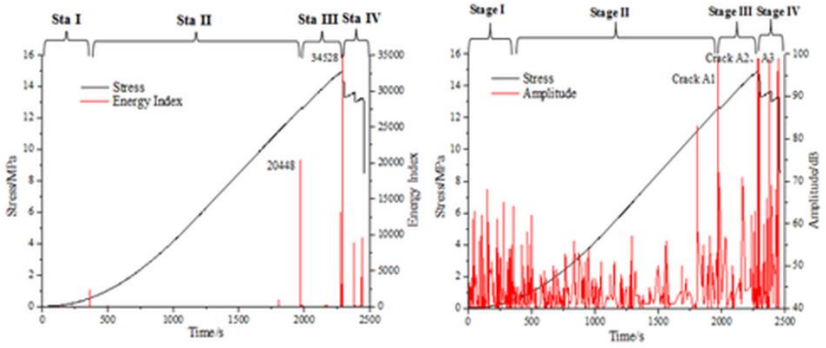

(a) Specimen1-1(l =30 mm)

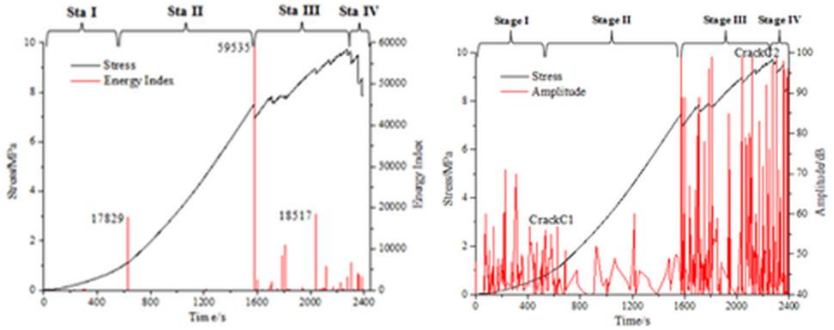

(b) Specimen 2-1 (l =40 mm)

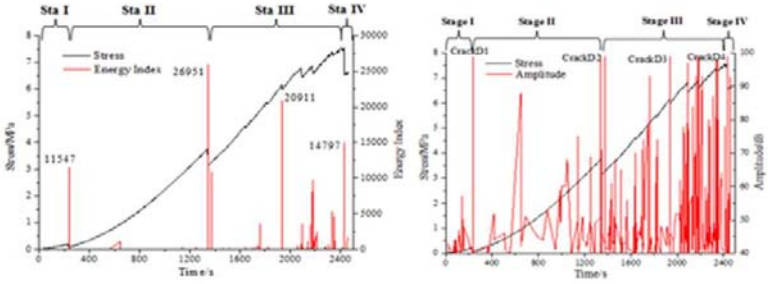

(c) Specimen 3-2 (l =50 mm）

Fig. 6. Acoustic Emission Characteristic Curve. Notes: the monitored acoustic emission energy signals were the relative energy without dimension

As shown in Figure 6, the compression of the rock-like specimen with edge crack can be divided into 4 stages namely initial compaction stage, elasticity stage, macro extension of crack stage and specimen failure stage as described below.

(1) Initial compaction stage (Stage I): as a rock-like material is homogeneous, with few air bubbles and defects and relatively dense structure, the stress-time curve is rather flat.

The pre-existing open crack in the specimen was deforming with stress and no new crack started. The acoustic emission signals were mainly caused by the closure of the open crack under pressure, with relatively low energy and magnitude.

(2) Elasticity stage (Stage II): at this stage the stress-time curve followed Hooke's law, exhibiting linear growth for a long period of time. Under the initial pressure, the pre-existing crack within the specimen closed, which creates stronger contacting forces and higher friction on the crack surface. Hence propagation of the pre-existing crack and development of new crack were constrained. In result, no new crack started in the specimen, and acoustic emission signals were weak.

(3) Macro extension of crack stage (Stage III): when the stress began to have "stepwise" change, new crack started and extended around the tip of the pre-existing crack, mainly in the form of wing tension crack. With load continuously increasing, the number and extension length of the new cracks kept growing, causing the AE energy and the magnitude to fluctuate suddenly. At this stage the acoustic emission signals became very active.

(4) Specimen failure stage (Stage IV): when the stress reached peak strength, the cracks extended to boundaries around them and eventually connected to each other around the pre-existing cracks. At this stage, the AE energy and the magnitude changed wildly, with stronger acoustic signals. Then the stress curve of the specimen descended rapidly and the specimen is disintegrated.

In summary, the following characteristics can be found for the crack propagation and its acoustic emission in the groups of specimens tested: (1) Wing tension crack firstly appeared in the specimen at the tip of the pre-existing crack, with an average cracking angle as 84.6°from horizontal direction and propagation angle close to the loading direction. (2) With the width of the edge crack increasing, the uniaxial compressive strength and the crack initiation strength gradually decreased, the time of crack initiation was changed from the end of the elasticity stage to the end of the initial compaction stage, which is earlier. (3) At the period of stress not pulse, the acoustic emission signals from the specimen were weak, with lower AE energy value and magnitude, suggesting that there was no or only minor crack occurring within it. When the stress changed in "stepwise" manner, the specimen produced much stronger acoustic emission signals with rapidly increasing energy value and magnitude, indicating the development of macro crack. (4) When the rock-like materials with edge cracks were applied with uniaxial compression, primarily wing, anti-wing and secondary tension cracks started from the tip of the pre-existing crack, and eventually crack extended into the crack-free region and then connected to each other and joined the pre-existing crack, resulting in tensile fracture in "J" shape or "reverse J" shape and causing the specimen to fail for tension.

4 Implication of the Study Results to Mining

As we know, the NO.16 coal seam flood was an incident that began on Monday, March 1, 2010, when a large amount of water flooded the Luotuoshan coal mine in the Inner Mongolia Autonomous Region of China. The roof of NO.16 coal seam is sandstone and mudstone, and the floor of that is mudstone and limestone. With the increase of tunnelling distance, the damage range of floor was enlarged and hidden structure developed by mining, as shown in Figure 7 (a) to (c).

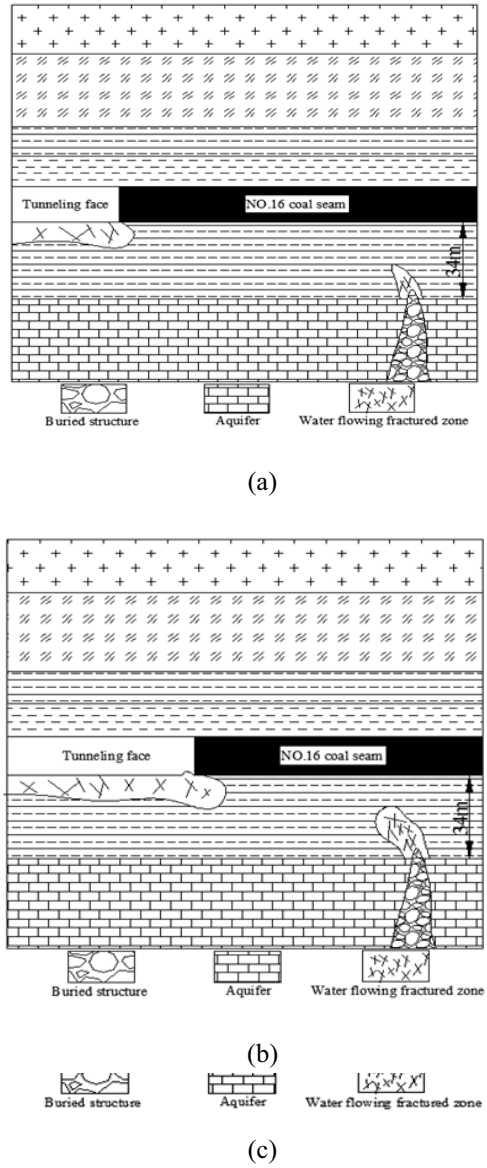

Fig. 7. The schematic diagram of Luotuoshan coal mine flood

After mining of coal seam, the roof stratum may collapse, bend or sink. The dynamic loading force produced by the movement of the roof stratum is applied on the coal rock body ahead of the mining face, damaging coal rock body and weakening its water resistance. Under the combined effect of the abutment pressure on the top and the confined water within the floor, the pre-existing cracks in the floor strata will further fracture and extend, significantly reducing the thickness of the aquitard in the floor and its water resisting capacity. The confined water can penetrate into the coal rock body ahead of the mining face through the damage zone created by the extension of pre-existing crack (or mining panel) and enter into the mining panel, causing water inrush into the mining face floor. Further, the principle of the Luotuoshan coal mine flood can be shown as Figure 8. In Figure 8, the inrush channel depicted in the figure essentially resembles with the anti-wing

tension cracks A2, B1 and C2 as depicted in Figure 5 (a) to (c). Hence the water inrush from the floor ahead of the mining face can be explained well with the propagation mechanisms for edge crack under vertical load.

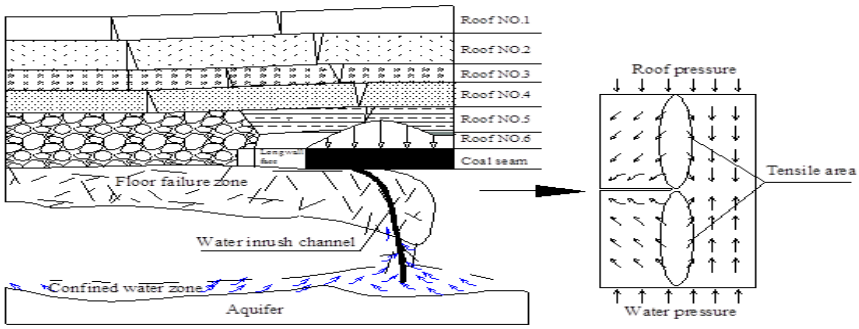

Fig. 8. Mechanism for inrush on the floor ahead of the coal mining face

Notes: the left of the figure depicts the seam roof, the damaged scope of the floor and the intrusion belt of the confined water, with the blue arrow indicating the flow direction of the confined water and the black bold line indicating the inrush channel. The part circled by dot line can be simplified into the right part of the figure. The oval part on right represents the tensile region of the specimen when it is under pressure, and the pre-existing crack at the center can be deemed as the coal mining face.

5 Conclusions

Under uniaxial compression, tension crack firstly appeared in the rock-like specimen with pre-existing edge crack at the tip of its pre-existing crack, with an average crack initiation angle of 84.6°, and it propagated rapidly in an angle close to the loading direction to the upper and lower ends of the specimen. With the width of the pre-existing crack increasing, the uniaxial compressive strength and the crack initiation strength of specimen decreased gradually. When the load reached the specimen's peak strength, anti-wing and secondary tension cracks started and crack extended into the crack-free region and then connected to the pre-existing crack, resulting in tensile fracture in "J" shape or "reverse J" shape and causing the specimen to fail in tension.

At the period of stress not pulse, the acoustic emission signals from the specimen were weak, with lower AE energy value and magnitude, suggesting that there was no or only minor crack occurring. When the stress changed in "stepwise" manner, the specimen produced stronger acoustic emission signals with rapidly increasing energy value and magnitude, indicating the development of macro crack.

The propagation mechanism of pre-existing edge crack under pressure can well explain the inrush on the floor ahead of the mining face. By comparing the propagation path of the anti-wing tension crack and the path of the inrush on the floor ahead of the mining face, it can be found that they share a strong similarity as there was tensile region formed within the floor rock under the effect of compressive load, so that the confined water can penetrate into the mining face along the tension damage zone, causing water inrush disaster.

6 Acknowledgements

This research was financially supported by the Shandong Provincial Natural Foundation (ZR2018LE008), Doctoral Research Foundation of Liaocheng University (318051701), General research project of teaching reform in Shandong Province (Z2016M044), Shandong graduate education quality improvement plan project (SDYJG19062), Research

Fund of Liaocheng University (318011901), National Natural Science Foundation of China (51974173), Key research and development plan of Shandong Province (2019GSF111024) and Shandong Province's Taishan Scholar Talent Team Support Plan for Advantaged & Unique Discipline Areas.

References

1. B. Shen, O. Stephansson, H. Einstein, Journal of Geophysical Research, **100**, 6, 5975 (1995).
2. W. F. Brace, E. G. Bombolakis, Journal of Geophysical Research, **68**, 12, 3709 (1963).
3. Y. S. Chen, L. I. Ning, H. Xin, Chinese Journal of Rock Mechanics and Engineering, **24**, 15, 2665 (2005).
4. W. Z. Chen, P. S. Chen, W. Hui, Rock and Soil Mechanics, **32**, 573 (2011).
5. E. Smith, International Journal of Solids and Structures, **17**, 6, 631 (1981).
6. F. Feng, S. J. Chen, D. Y. Li, S. T. Hu, W. P. Huang, B. Li, Energy Science and Engineering, **7**, 6, 2264 (2019).
7. F. Feng, X. B. Li, J. Rostami, D. X. Peng, D. Y. Li, K. Du, International Journal of Geomechanics, **19,** 4, 04019005 (2019).
8. S. Li, T. Li, G. Wang, et al, Chinese Journal of Rock Mechanics and Engineering, **26**, 3, 484 (2007).
9. Luis Arnaldo Mejía Camones, Eurípedes do Amaral Vargas Jr., et al, Engineering Geology, **153**, 80 (2013).
10. R.H.C. Wong, P. Lin, C.A. Tang, Mechanics of Materials, **38**, 1-2, 142 (2006).
11. B.Shen, O.Stephansson, M.Rinne, et.al, International Journal of Geomechanics, **1**, 4, 302 (2011).
12. B. Shen, J. Shi, International Journal of Rock Mechanics and Mining Sciences, **88**, 206 (2016).
13. B. Shen, B. Zhang, S. Zhang, B. Chen, Journal of Shandong University of Science and Technology(Natural Science), **39,** 2, 4452 (2020).
14. W. Sun, S. Zhang, W. Guo, W. Liu, Mine Water & the Environment, **36**, 2, 1 (2017).
15. C. A. Tang, L. X. Tang, L. I. Lian-Chong, et al, Chinese Journal of Geotechnical Engineering, **29**, 1, 71 (2007).
16. Y. Q. Wang, Z. C. Feng, H. Q. Guo, et al, Rock and Soil Mechanics, **34**, 9, 2534 (2013).
17. F. Y. Xue, C. J. Guan, K. Arakawa, et al, Polymer Testing, **21**, 8, 933 (2002).
18. G. S. Yang, H. Liu, Journal of China Coal Society, **32**, 5, 463 (2007).
19. S. Zhang, W. Guo, Y. Li, W. Sun, D. Yin, Mine Water & the Environment, **36**, 443 (2017).
20. S. Zhang, B.T. Shen, Y. Li, Geofluids, **1**, 1, (2019).
21. Z. Cheng, J. Tian, M. Hiroshi, et al, Chinese Journal of Rock Mechanics and Engineering, **34**, 4, 763 (2015).
22. X. D. Zhao, J. P. Liu, L. I. Yuan-Hui, et al, Chinese Journal of Geotechnical Engineering, **30**, 10, 1472 (2008).
23. Z. D. Zhu, H. X. Lin, Y. L. Sun, et al, Rock and Soil Mechanics, **37**, 4, 913 (2016).